J|A|C|S ARTICLES

Published on Web 03/30/2009

H-Atom Position as Pattern-Determining Factor in Arenethiol Films

Ki-Young Kwon,[†,‡] Greg Pawin,[†,§] Kin L. Wong,[†,§] Eric Peters,[†] Daeho Kim,[†] Sampyo Hong,[||] Talat S. Rahman,[||] Michael Marsella,[†] and Ludwig Bartels*[,†]

Pierce Hall/Department of Chemistry, University of California−Riverside, Riverside, California 92521, Physical Biosciences Division, Lawrence Berkeley National Laboratory, Berkeley, California 94720, Departments of Chemistry/Electrical Engineering, University of California−Los Angeles, Los Angeles, California 90095, and Department of Physics, University of Central Florida, Orlando, Florida 32816

Received December 2, 2008; E-mail: Ludwig.Bartels@ucr.edu

Abstract: The evolution of a low coverage of benzenethiol molecules on Cu(111) during annealing shows the prevalence of S···H hydrogen bonds involving hydrogen atoms in the ortho position. The row and pattern formation of (methylated) anthracenethiols indicates intermolecular interactions in which hydrogen atoms at the terminal position of the aromatic moiety dominate. In combination, this leads to the notion that pattern formation in classes of arenethiol molecules is each governed by optimization of the intermolecular interactions of the hydrogen atom at one particular position on the arene. This may provide a general guiding principle for the design of arenethiol films.

1. Introduction

The conducting and dynamic properties of (thiolated) arenes on coinage metal surfaces have been studied intensely because these compounds feature both outstanding facility in the fabrication of molecular-scale contacts (i)[1,2] and unique diffusive properties (ii).[3] Arenes stacked parallel to the surface have been suggested for charge injection at metal electrodes (iii).[4] While for application i the molecule is generally lifted at least partially from the substrate and the interaction of the thiol group with the substrate is paramount, ii relies on a delicate interplay between sulfur and arene substrate interactions and iii, for which generally unthiolated arenes are used, crucially depends on the arene−substrate interaction and ensuing columnar stacking pattern. Despite these technological promises there have been very few studies addressing pattern formation in such films in a systematic fashion, i.e., addressing more than 1 or 2 related compounds. While many interesting phenomena have been observed already, generally not a sufficient number of related molecules were investigated to glean general rules. In contrast, pattern formation of alkanethiols on coinage metal surfaces (in particular gold) has been addressed extensively, mainly because those systems provide a convenient path for self-assembled functionalization.[5,6]

Intermolecular hydrogen bonds have emerged as important pattern-determining factors,[7−19] even for systems in which conventional X−H···X′ bonding (with X and X′ = O, N, F) cannot occur.[20−24] They provide an alternative to pattern control

[†] University of California−Riverside.
[‡] Lawrence Berkeley National Laboratory.
[§] University of California−Los Angeles.
[||] University of Central Florida.

(1) Chen, F.; Hihath, J.; Huang, Z. F.; Li, X. L.; Tao, N. J. *Annu. Rev. Phys. Chem.* **2007**, *58*, 535–564.
(2) Heath, J. R.; Ratner, M. A. *Phys. Today* **2003**, *56* (5), 43–49.
(3) Kwon, K. Y.; Wong, K. L.; Pawin, G.; Bartels, L.; Stolbov, S.; Rahman, T. S. *Phys. Rev. Lett.* **2005**, *95* (16), 166101.
(4) Dimitrakopoulos, C. D.; Malenfant, P. R. L. *Adv. Mater.* **2002**, *14* (2), 99–103.
(5) Love, J. C.; Estroff, L. A.; Kriebel, J. K.; Nuzzo, R. G.; Whitesides, G. M. *Chem. Rev.* **2005**, *105* (4), 1103–1169.
(6) Poirier, G. E. *Chem. Rev.* **1997**, *97* (4), 1117–1127.
(7) Theobald, J. A.; Oxtoby, N. S.; Phillips, M. A.; Champness, N. R.; Beton, P. H. *Nature* **2003**, *424* (6952), 1029–1031.
(8) Xu, B.; Tao, C. G.; Williams, E. D.; Reutt-Robey, J. E. *J. Am. Chem. Soc.* **2006**, *128* (26), 8493–8499.
(9) Llanes-Pallas, A.; Matena, M.; Jung, T.; Prato, M.; Stohr, M.; Bonifazi, D. *Angew. Chem.* **2008**, *47* (40), 7726–7730.
(10) Otero, R.; Schock, M.; Molina, L. M.; Laegsgaard, E.; Stensgaard, I.; Hammer, B.; Besenbacher, F. *Angew. Chem.* **2005**, *44* (15), 2270–2275.
(11) Lackinger, M.; Griessl, S.; Kampschulte, L.; Jamitzky, F.; Heckl, W. M. *Small* **2005**, *1* (5), 532–539.
(12) De Feyter, S.; De Schryver, F. C. *Chem. Soc. Rev.* **2003**, *32* (3), 139–150.
(13) Keeling, D. L.; Oxtoby, N. S.; Wilson, C.; Humphry, M. J.; Champness, N. R.; Beton, P. H. *Nano Lett.* **2003**, *3* (1), 9–12.
(14) Weckesser, J.; De Vita, A.; Barth, J. V.; Cai, C.; Kern, K. *Phys. Rev. Lett.* **2001**, *87* (096101).
(15) Barth, J. V.; Weckesser, J.; Cai, C. Z.; Gunter, P.; Burgi, L.; Jeandupeux, O.; Kern, K. *Angew. Chem.* **2000**, *39* (7), 1230–1234.
(16) Nakagawa, T.; Tanaka, H.; Kawai, T. *Surf. Sci.* **1997**, *370* (1), L144–L148.
(17) Payer, D.; Comisso, A.; Dmitriev, S.; Strunskus, T.; Lin, N.; Wol, C.; DeVita, C.; Barth, J.; Kern, K. *Chem.-Eur. J.* **2007**, *13* (14), 3900–3906.
(18) Zhang, X.; Yan, C. J.; Pan, G. B.; Zhang, R. Q.; Wan, L. J. *J. Phys. Chem. C* **2007**, *111* (37), 13851–13854.
(19) Rohde, D.; Yan, C. J.; Wan, L. J. *Langmuir* **2006**, *22* (10), 4750–4757.
(20) Pawin, G.; Solanki, U.; Kwon, K. Y.; Wong, K. L.; Lin, X.; Jiao, T.; Bartels, L. *J. Am. Chem. Soc.* **2007**, *129*, 12056–12057.
(21) Pawin, G.; Wong, K. L.; Kwon, K. Y.; Bartels, L. *Science* **2006**, *313* (5789), 961–962.
(22) Desiraju, G. R. *Acc. Chem. Res.* **2002**, *35* (7), 565–573.
(23) Desiraju, G. R. *Chem. Commun.* **2005**, (24), 2995–3001.

 10.1021/ja809417k CCC: $40.75

Scheme 1. BT (I), BDT (II), AT (III), ADT (IV), MADT (V), and DMADT (VI)

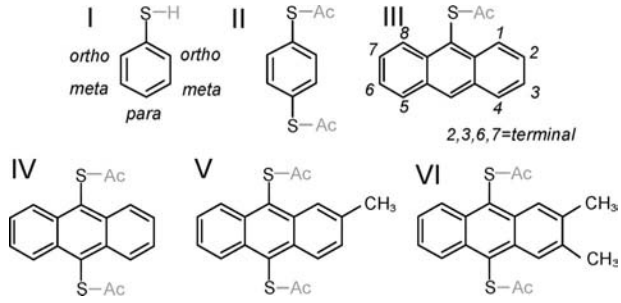

by means of substrate reconstruction,[25] electrostatic interaction,[26,27] or surface coordination chemistry,[29] yet there is no comprehensive understanding which hydrogen atoms feature most prominently in them. Hydrogen bonding is known to depend delicately on the electronic structure, bond length, and bond angle, a problem reappearing in many current disciplines of chemistry from surface science to proteomics.

In this study we contrast the pattern formation (or the absence thereof) in coverages of benzenethiol (I, BT), benzene-1,4-dithiol (II, BDT), anthracene-9-thiol (III, AT), anthracene-9,10-dithiol (IV, ADT),[3] 2-methylanthracene-9,10-dithiol (V, MADT), and 2,3-dimethylanthracene-9,10-dithiol (VI, DMADT) adsorbed on Cu(111). These experiments were performed in ultrahigh vacuum and use scanning tunneling microscopy at cryogenic temperatures.

2. Methods

2.1. Imaging. We used a home-built variable-temperature scanning tunneling microscope (STM) operated in ultrahigh vacuum. Cu(111) sample preparation involved sputtering (Ar^+, 3 kV) and annealing of a single crystal followed by cooling to liquid nitrogen temperatures within the STM. Deposition onto the cold sample occurred for anthracene-based species from a glass capillary attached to the vacuum chamber through a gate valve in a line-of-sight fashion while controlling the deposition rate through measurement of the pressure in the vacuum chamber. Benzene-based species were dosed through a needle valve due to their higher vapor pressure. BDT and all anthracene-based species were acetyl protected prior to deposition (see Synthetic section below) and required postdeposition anneal of the sample to room temperature in order to remove protecting groups, which was confirmed by mass spectrometry.

2.2. Theoretical. Density functional theory (DFT) calculations of the electronic and geometric structures and interaction energies of all molecules on Cu(111) were carried out using the Vienna Ab-Initio Simulation Package (VASP)[29] implementing the generalized gradient approximation (GGA) for the exchange-correlation functional[30] and the plane-wave pseudopotential method.[31] Ultrasoft pseudopotentials[32] were used for all atoms in the system. The cutoff energy for the plane-wave expansion is taken to be 400 eV, and a single k point is used in Brillouin zone sampling to obtain converged results for the total energy of the system. All supercells have three substrate (Cu) layers so as to keep the total number of substrate atoms in the supercell to approximately 100 for computational feasibility. During lattice relaxation, all adsorbate and top-layer substrate atoms were allowed to move in all directions. The structures and free energies that are shown in this study result from relaxation of the forces acting on each atom to better than 0.02 eV/Å. Calculations of the molecular structure in the gas phase use BLYP/6-31G* in Spartan.[33]

2.3. Synthetic. The synthesis of AT, MADT, and DMADT follows the synthesis of 9,10-dithioacethylanthracene described in ref 3, its Supporting Information, and references therein. In a nutshell, we used appropriate oxygen-based precursors and converted them with Lawesson's reagent to the polymerized or dimerized anthracenedisulfide, whose sulfur atoms we subsequently esterfied via reduction with sodium borohydride followed by in situ addition of acetic anhydride. BDT was obtained from Alfa Aesar, and we acetyl protected it to avoid polymerization during deposition.

All reactions were carried out under N_2 and Ar gas, and all glassware was dried in an oven at 100 °C. All solvents (HPLC grade) were used without purification. The reactions were identified by thin layer chromatography using UV light. The compounds were purified by column chromatography (particle size 230−400 mesh).

3. Results

3.1. Benzene Derivates. The Yates' group showed that BT is capable of extracting atoms from a gold surface to form BT−Au−BT bridges similar to those on gold nanoparticles.[34,35] BT adsorbs on Cu(111) under hydrogen abstraction (at temperatures as low as 40 K)[36] with its sulfur anchor close to a substrate bridge site, i.e., without extraction of a substrate atom. BT has a diffusion barrier of 150 meV, and it is able to rotate at 120−130 meV barrier through two sets of three equivalent adsites with slightly different binding energies (see Figure 1a).[37]

In this study we followed the evolution of a number of BT molecules while increasing the substrate temperature from 50 to 90 K (i.e., by ∼70%). The Supporting Information contains a movie showing >700 images from this series acquired over >24 h. Initially, we observe a number of odd-shaped molecular aggregates, isolated molecules (yellow in Figure 1b), dimers (red), trimers, and tetramers. Unsurprisingly, isolated molecules become mobile first and attach to nearby islands. Subsequently, dimers become mobile and start to rearrange. Analysis of a large number of STM images at high resolution and ∼60 K temperature reveals the distribution of dimers shown in Figure 2c. The majority of dimers are found to interact by placing the sulfur atom of one molecule in the vicinity of an H_{ortho} of another molecule. In most cases (purple portion), both molecules adsorb in the preferred adsorption configuration (left in Figure 1a), yet in some cases at least one of the molecules occupies the less favored one (yellow portion). A significantly smaller number of molecules are found to interact via the H_{meta} and even fewer via H_{para}.

We performed DFT calculations in which we placed two BT molecules on a sufficiently extended Cu(111) slab at >10

(24) Yokoyama, T.; Yokoyama, S.; Kamikado, T.; Okuno, Y.; Mashiko, S. *Nature* **2001**, *413* (6856), 619–621.
(25) Barth, J. V.; Brune, H.; Ertl, G.; Behm, R. J. *Phys. Rev. B* **1990**, *42* (15), 9307–9318.
(26) Muller, T.; Werblowsky, T. L.; Florio, G. M.; Berne, B. J.; Flynn, G. W. *Proc. Natl. Acad. Sci. U.S.A.* **2005**, *102* (15), 5315–5322.
(27) Wong, K.; Kwon, K.; Rao, B.; Liu, A.; Bartels, L. *J. Am. Chem. Soc.* **2004**, *126* (25), 7762–7763.
(28) Barth, J. V.; Costantini, G.; Kern, K. *Nature* **2005**, *437* (7059), 671–679.
(29) Kresse, G.; Hafner, J. *Phys. Rev. B* **1993**, *47* (1), 558–561.
(30) Perdew, J. P.; Wang, Y. *Phys. Rev. B* **1992**, *45* (23), 13244–13249.
(31) Payne, M. C.; Teter, M. P.; Allan, D. C.; Arias, T. A.; Joannopoulos, J. D. *Rev. Mod. Phys.* **1992**, *64* (4), 1045–1097.
(32) Vanderbilt, D. *Phys. Rev. B* **1990**, *41* (11), 7892–7895.
(33) *Spartan 06*; Wavefunction Inc.: Irvine, CA, 2006.
(34) Jadzinsky, P. D.; Calero, G.; Ackerson, C. J.; Bushnell, D. A.; Kornberg, R. D. *Science* **2007**, *318* (5849), 430–433.
(35) Maksymovych, P.; Yates, J. T. *J. Am. Chem. Soc.* **2008**, *130* (24), 7518–7519.
(36) Rao, B.; Kwon, K.; Liu, A.; Bartels, L. *Proc. Natl. Acad. Sci. U.S.A.* **2004**, *101* (52), 17920.
(37) Wong, K.; Kwon, K. Y.; Bartels, L. *Appl. Phys. Lett.* **2006**, *88*, 183106.

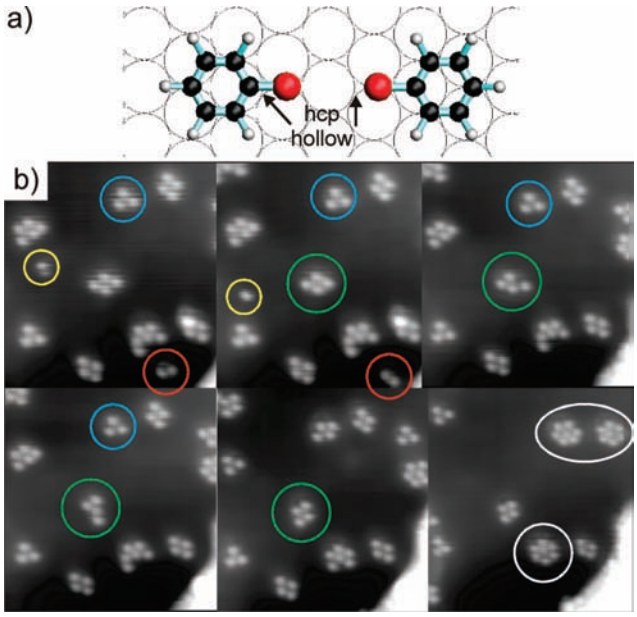

Figure 1. (a) BT and its adpositions on Cu(111) from ref 37. (b) Sequence of STM images (−1.4 V, 34 pA, 180 Å × 190 Å) during the annealing of BT/Cu(111) from 50 to 90 K. Initially individual molecules (yellow) become mobile followed by dimers (red). Trimers (blue) are very stable and often attach another molecule (green) on the periphery, which can rearrange itself facilely. Ultimately, the majority of molecules form stable heptamers.

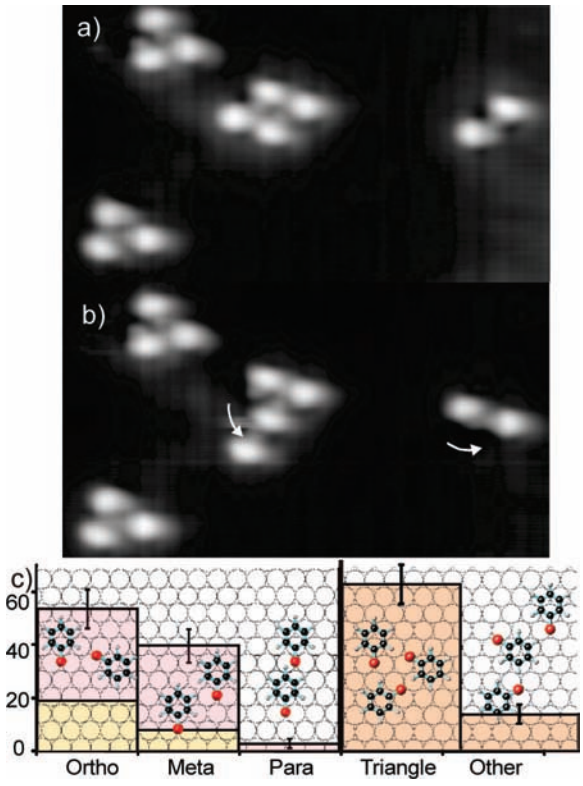

Figure 2. (a and b) STM images (140 Å × 77 Å) resolving the benzene ring (bright) and sulfur anchor (gray shoulder) of BT. Two triangular trimers and rearrangement of a tetramer and an H_{ortho}-interacting dimer are visible. (c) Statistical evaluation of dimers shows that the majority of them interacts via H_{ortho} followed by H_{meta}. Trimers tend to form triangles (as in panels a,b) rather than any other pattern (not only the one shown).

different relative orientations and separations, including various ones that allow for interaction via H_{ortho}, H_{meta}, and H_{para}. For each of the three interactions, the background of Figure 2c shows

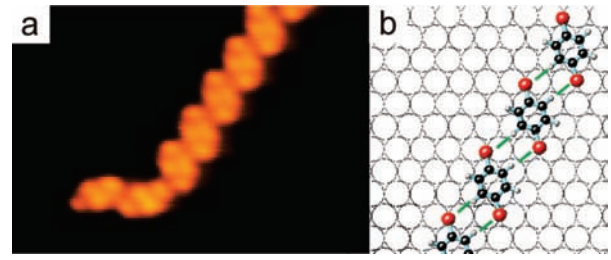

Figure 3. (a) Row of BDT molecules interacting via H_{ortho} (−2.0 V, 31 pA, 67 Å × 46 Å) and corresponding model (b).

the configuration associated with the most pronounced lowering of the total free energy by 102, 88, and 42 meV compared to separated molecules, respectively. These results show a wide distribution of S···H−C bond lengths of 3.6, 3.9, and 3.1 Å, respectively. The sequence of interaction energies corroborates our experimental observation of the dominance of the H_{ortho} atom in intermolecular interaction, and it is in good agreement with previous work on fluorinated species.[19,38]

Upon further anneal of the molecular population of Figure 1, triangular trimers (most commonly of the kind shown in the background of Figure 2c) are found (blue circle), yet also other trimers (see Figure 2a,b) exist. Figure 2c compares the abundance of triangular trimers to that of trimers of all other shapes (i.e., not only the linear one shown). It should be noted that trimers composed of a closed loop of both H_{ortho}- and H_{meta}-interacting molecules are sterically possible, yet the latter are rarely observed. During our measurements, trimers frequently attach another molecule that subsequently changes position and configurations quite rapidly (green circle), leading us to interpret most tetramers as a stable trimer with an additional molecule attached. No tetramers with a 'circular' interaction pattern (like for the pictured trimer) have been observed. Ultimately, virtually the entire population of BT is converted into heptamers that incorporate both H_{ortho} and H_{meta} interactions. Similar to the trimers, these heptamers shield their sulfur atoms from interacting with additional molecules. Consequently, they do not form the nucleus for larger ordered aggregates, and no ordered surface coverage emerges.

The evolution of the BT coverages is reminiscent of Oswald ripening, a common feature in, e.g., metal epitaxy, which has also been observed for molecules.[39] Due to the anisotropic nature[40] of the BT−BT interaction epitomized by the dominance of H_{ortho} in intermolecular interactions (in contrast to the isotropic interactions of, e.g., metal atoms), we observe the formation of stable 'magic' clusters at relatively small cluster size.[41]

Is the dominance of one particular hydrogen atom a general feature of intermolecular interaction in arenethiol films? To address this question, we proceed in two directions: (i) conversion of all BT hydrogen atoms to H_{ortho} by addition of a second thiol group (resulting in BDT) and (ii) extension of the arene moiety to anthracene.

STM images of a low coverage of BDT show the formation of chains (Figure 3), in which each sulfur interacts with an H_{ortho}

(38) Prins, L. J.; Reinhoudt, D. N.; Timmerman, P. *Angew. Chem.* **2001**, *40* (13), 2383–2426.
(39) Barrena, E.; Ocal, C.; Salmeron, M. *J. Chem. Phys.* **1999**, *111* (21), 9797–9802.
(40) Morgenstern, K.; Rosenfeld, G.; Laegsgaard, E.; Besenbacher, F.; Comsa, G. *Phys. Rev. Lett.* **1998**, *80* (3), 556–559.
(41) Bohringer, M.; Morgenstern, K.; Schneider, W.; Berndt, R. *J. Phys.: Condens. Matter* **1999**, *11* (49), 9871–9878.

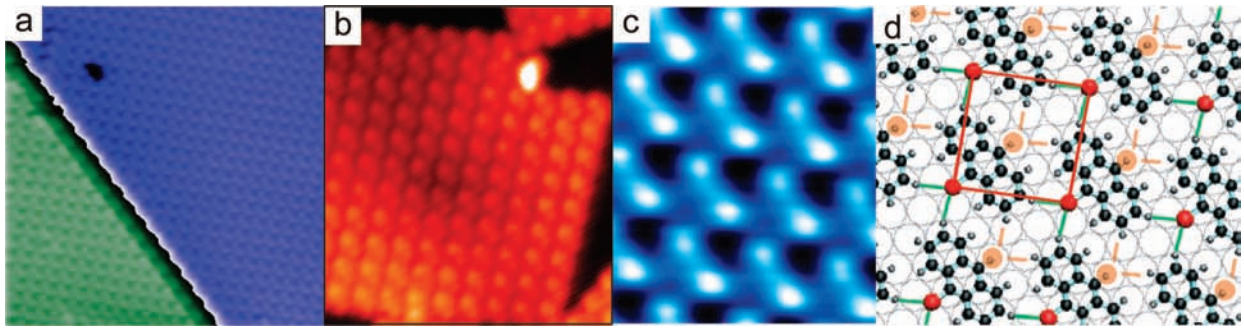

Figure 4. (a and b) STM images (−0.9 V, 94 pA, 200 Å × 200 Å and −2.3 V, 79 pA, 96 Å × 110 Å) of AT and ADT on Cu(111), respectively, showing successive molecular rows in antiphase (zoomed in at panel c, 27 Å × 32 Å). (d) molecular model of the pattern with unit cell and intermolecular bonds for AT (green) and ADT (orange) indicated.

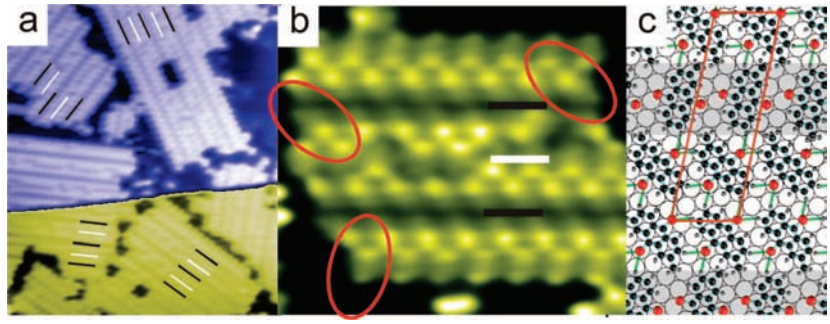

Figure 5. (a and b) MADT islands (−1.5 V, 85 pA, 360 Å × 410 Å and −2.2 V, 49 pA, 86 Å × 86 Å) showing double rows of molecules that present their protruding methyl groups to the outside. The inside of these rows appears as a depression running along the row direction. It is highlighted with a black bar in panels a and b and corresponds to the unshaded area of panel c. These double rows are separated by a single row of molecules at a different yet equivalent surface orientation presenting their methyl groups to either side randomly causing a disordered appearance of this row (highlighted with a white bar; shaded region in panel c). The orientation of the molecules is visible at the row edges indicated with ellipses.

atom of a neighboring molecule. BDT adsorbs with both sulfur atoms near bridge sites, which positions the arene ring at an asymmetric configuration with regard to the substrate (in contrast to BT, Figure 1a), thereby allowing H_{ortho} interactions between parallelly adsorbed molecules. The importance of H_{ortho} interactions is further underlined by the fact that upon increase of the BDT coverage a variety of patterns emerge that are characterized by interwoven rows similar to the H_{ortho} rows shown in Figure 3a.

3.2. Anthracene Derivates. Can we find a similar prevalence of one particular hydrogen atom in intermolecular interaction of a different arene backbone? To strengthen the notion that arenethiol pattern formation is determined by the optimization of the intramolecular interaction of the hydrogen atom in one particular position on the ring, we explore anthracenethiols.

AT (the anthracene counterpart of BT) forms a surface pattern with an almost square $[^{3}_{1}\ ^{3}_{-4}]$ lattice (Figure 4a,c): each molecule adsorbs at a position and an orientation similar to BT while aligning the anthracene moieties in parallel rows, with successive rows offset by 2.5 lattice vectors along the row direction (Figure 4d). This places the sulfur atom of one molecule in close proximity to the hydrogen atoms in 3 and 6 positions of the two molecules in the adjacent row. On the basis of this observation, we explore whether the hydrogen in position 3, or more generally the terminal hydrogen atom of the anthracene system, is the one that dominates the intermolecular interaction (and thus determines the film pattern) for anthracenethiols on Cu(111).

Addition of a second thiol group to AT at the opposite side of the ring results in ADT, which forms the same $[^{3}_{1}\ ^{3}_{-4}]$ lattice as AT (Figure 4b). Due to the presence of sulfur atoms on both sides of ADT, all terminal hydrogen atoms are equivalent (save for a difference in adsite of the sulfur atoms),[3] and they are all involved in intermolecular interactions (Figure 4d), yet the inequivalent hydrogen atoms in positions 1, 4, 5, and 8 do not participate.

We further explore which impact introduction of steric hindrance (by means of methyl groups) has on the film pattern. In particular, we wish to elucidate whether the dominance of the original H_{term}-based intermolecular interaction persists, forcing the film to adopt a more complicated geometry to accommodate both the interaction and the steric hindrance at the same time or whether the steric hindrance suppresses the original kind of interaction permitting another kind of intermolecular interaction to shape the film pattern.

Replacement of one of the terminal hydrogen atoms with methyl results in MADT. Due to its lower symmetry, an MADT film (Figure 5a,b) adopts a more complex pattern characterized by alternating rows of linear depressions that appears to be flanked by ordered rows of protrusions (highlighted black in Figure 5a) and disordered zig-zagging depressions (highlighted white in Figure 5a). At higher magnification (Figure 5b) it becomes apparent that the first kind of linear depression reflects a double row of molecules pointing their protruding methyl groups to the outside. This allows their anthracene and thiol moieties to interact in the inside of the row as if no substitution were present (unshaded portion of Figure 5c). Due to the lack of methyl-induced protrusion, this portion of the film appears as an indentation. These double rows of molecules are separated from one another by a row of molecules whose anthracene moiety is rotated by 120° with regard to those in the double rows (resulting in an equivalent adsite due to the 3-fold

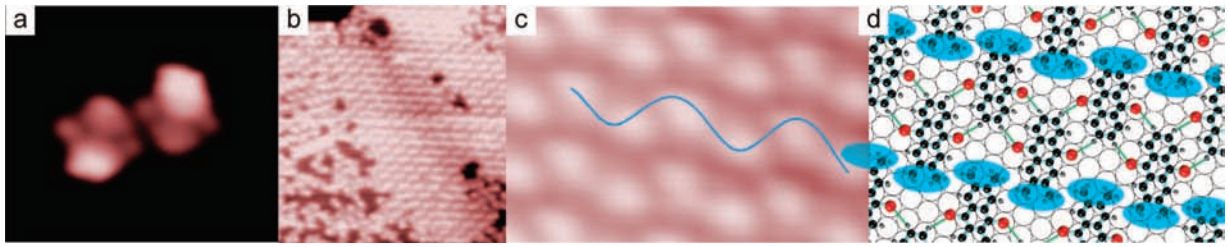

Figure 6. (a, b, and c) Individual DMADT molecules and film pattern (−0.4 V, 45 pA, 33 Å × 28 Å; −1.0 V, 78 pA, 280 Å × 290 Å; −0.4 V, 45 pA, 56 Å × 36 Å) consisting of parallel molecular rows with alternating orientation of the methyl groups leading to a wavy pattern (blue lines) of protrusions representing the methyl groups (d).

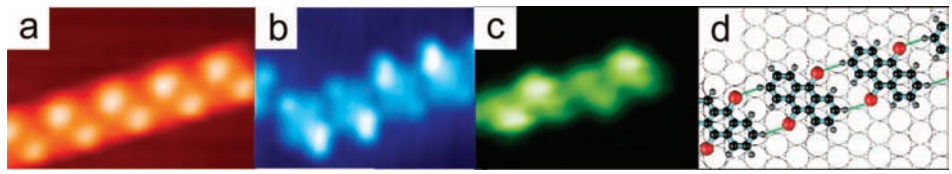

Figure 7. STM images of rows of (a) ADT, (b) MADT, (c) DMADT (−1.5 V, 79 pA, 52 Å × 28 Å; −1.5 V, 85 pA, 46 Å × 34 Å; −3.0 V, 41 pA, 44 Å × 32 Å), and (d) model showing the molecular setup and hydrogen bonding in this configuration. The methylated species adopt the same pattern.

symmetry of the Cu(111) substrate). These molecules interact with one another in the same way as those in the double rows, and they point their extra methyl group at random toward either one or the other of the adjacent double rows, giving rise to the disordered appearance of this row. In combination, there are three molecules per unit cell, which can be represented in matrix notation as $[^{1}_{1}\ ^{1}_{-3}\ _{4}]$. The H_{term} interactions in this film are highlighted Figure 5c; counting their number it becomes apparent that they are the dominant way of intermolecular interaction despite the low symmetry of the individual molecules.

Methyl substitution of all terminal hydrogen atoms on one side of ADT leads to DMADT, which forms a pattern (Figure 6a−c) reminiscent of A(D)T: the molecules align their anthracene moieties in rows with successive rows pointing the methyl groups in opposite direction. Along the anthracene rows, the molecules are separated by one more substrate lattice spacing to accommodate the extra methyl groups. Adjacent rows arrange the methyl groups to opposite sides, so that the methyl groups form a line meandering perpendicular to the row direction through the film (blue line), rendering the impression that an indentation (the unsubstituted side of the molecules) meanders in parallel. Counting the S···$H_{terminal}$ interactions indicated in green in Figure 6d, it becomes apparent that this film also favors this particular kind of intermolecular interaction.

Thus, we find films of four different anthracenethiol species adopting patterns tailored to optimize the intermolecular interactions of the hydrogen atom at the *terminal* position of the acene. Does this only occur in extended films, or is this interaction also dominant for small aggregates of molecules (like the H_{ortho}-based interaction in BT aggregates)? To answer this question, we also imaged low coverages of these molecules. Previous studies already showed row formation for ADT,[3,20] at a periodicity identical to the ADT film pattern, i.e., in these rows both sulfur atoms of one molecule interact with the $H_{terminal}$ atoms of their neighbors. MADT (Figure 7b) and DMADT (Figure 7c) form the same kind of row, with the extra methyl groups avoiding perturbation of the S···$H_{terminal}$ interaction by pointing to either side of the row at random (MADT) or alternatingly (DMADT), again highlighting the particular role of the terminal position for intermolecular interaction.

4. Discussion

The investigation of two and four members of two classes of arenethiols on Cu(111) reveals that for each class film patterns emerge that optimize the S···H−C intermolecular interaction in one particular position on the aromatic system. This suggests that once this position is identified for one particular molecular backbone and substrate, the film patterns of differently substituted molecules can be predicted. At this point the question remains to be answered, what is special about these particular hydrogen-atom positions.

Geometrically, H_{ortho} has the longest C−H bond in the molecule both in the gas phase and on the surface, suggesting that it is most prone to intermolecular interaction. Also, in terms of Lewis acid/base complexes, H_{para} lies at a node of the LUMO of BT. As such, HOMO−LUMO interactions should prefer $H_{ortho/meta}$. Indeed, a preference for H_{ortho} has been reported earlier for fluorine-containing compounds.[19,38] The case is less straightforward for anthracene derivates, where the $H_{terminal}$ bond is longer in calculations for the gas phase, but indistinct bond lengths are found in surface calculations.

Our DFT calculations of the surface-bound molecules find charge density at the hydrogen atoms of the molecules as shown in the top of Figure 8. The spectra show only occupied states, i.e., states below the Fermi level. Due to the node of the π system in the plane of the hydrogen atoms, no π-derived states are evident (including the HOMO). The highest energy feature with significant density at the hydrogen atom (marked I in Figure 8) derives from the d bands of the substrate, followed by several states stemming from the σ system of the aromatic moiety. Notably, the second (II) feature appears to be correlated with the propensity of an atom for taking part in intermolecular interaction, whereas the third (III) feature, in particular for ADT, is dominant, if no hydrogen bonding occurs based on the corresponding atom: for ADT, where we find interaction exclusively via H_{term} and not via the internal hydrogen atoms the ratio between the weights of feature II and III are 3.2 vs 0.07, respectively. For BT, where we find a more gradual preference for H_{ortho} over H_{meta} over $H_{para,}$ the ratios are 1.8 vs 1.6 vs 1.4. Why do these states affect the propensity of the hydrogen atoms for intermolecular interaction?

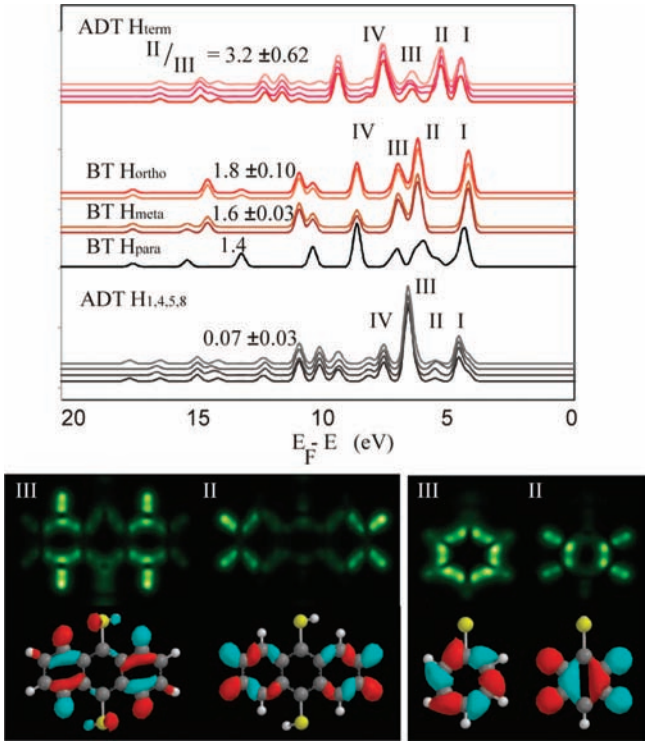

Figure 8. (top) Calculated density of states at the location of the hydrogen atoms. The ratio of the weight of states II and III (indicated error based on variation between atoms equivalent in the gas phase) correlates with the propensity of the atom in intermolecular interaction. (bottom) Charge density of states III and II for the adsorbed molecule (using energy intervals of 6.75−6.35, 5.43−5.03, 7.02−6.75, and 6.22−5.96 eV below E_F, respectively) and the corresponding gas-phase molecular orbitals (found at 6.6, 5.1, 5.9, and 5.0 eV below the HOMO).

The bottom panel of Figure 8 shows a projection of their extent. For comparison, the figure also shows the corresponding states as calculated for the gas phase, where the nodal structure can be calculated directly. The projections show that feature II corresponds to a σ orbital pointing to the periphery of the molecule for both BT and ADT. In contrast, feature III places more weight inside the molecule. As the availability of charge density at the periphery of a molecule is crucial for hydrogen-bond-based intermolecular interaction with its neighbors, these findings provide a quantum-level rational for the experimentally observed dominance of the intermolecular interaction of one particular hydrogen atom in each system. The prominent positions of these states in the electronic spectra suggest that the hydrogen-atom position dominating intermolecular interaction may be derived straightforward from theory rather than requiring any measurements at all.

5. Conclusion

We addressed several members of two families of arenethiols systematically and found that their film patterns are tailored to optimize the intermolecular interactions of the hydrogen atoms in particular positions on the arene and that this predominance of one position persists upon further inert or thiol substitution of the arene. In combination, our findings suggest that once for a class of arenes the dominant H-atom position is identified, the patterns of inertly substituted species can be predicted, at least on Cu(111). Moreover, the dominant position on the arene can be rationalized straightforwardly from DFT calculations of the adsorption configuration, and it is in good agreement with the conventional chemical behavior of the molecule, suggesting an even further degree of predictability of the molecular film patterns.

Acknowledgment. This work was supported by the U.S. Department of Energy under grants DE-FGO2-03ER15464 (Bartels)/DE-FG02-07ER15842 (Rahman) and the U.S. National Science Foundation 0647152 (Bartels/Marsella). Computational resources were made available by the San Diego Supercomputer Center.

Supporting Information Available: Movie of STM images pertinent to Figure 1. This material is available free of charge via the Internet at http://pubs.acs.org.

JA809417K